LAWRENCE
LIVERMORE
NATIONAL
LABORATORY

UCRL-JRNL-232549

A Proposal for High-resolution X-ray Imaging of Intermodal Cargo Containers for Fissionable Materials

B. Pohl, S. Prussin, J. Hall, J. Trebes, M.A. Descalle, B.J. Quiter

July 6, 2007

Journal of Applied Physics

Disclaimer

This document was prepared as an account of work sponsored by an agency of the United States Government. Neither the United States Government nor the University of California nor any of their employees, makes any warranty, express or implied, or assumes any legal liability or responsibility for the accuracy, completeness, or usefulness of any information, apparatus, product, or process disclosed, or represents that its use would not infringe privately owned rights. Reference herein to any specific commercial product, process, or service by trade name, trademark, manufacturer, or otherwise, does not necessarily constitute or imply its endorsement, recommendation, or favoring by the United States Government or the University of California. The views and opinions of authors expressed herein do not necessarily state or reflect those of the United States Government or the University of California, and shall not be used for advertising or product endorsement purposes.

A Proposal for High-resolution X-ray Imaging of Intermodal Cargo Containers for Fissionable Materials

by

B.J. Quiter[1], S.G. Prussin[1,2,*], B. Pohl[2], J. Hall[2], J. Trebes[2], G. Stone[2], and M.-A. Descalle[2]

[1]Department of Nuclear Engineering, University of California, Berkeley, California 94720
[2]Lawrence Livermore National Laboratory, Livermore, California 94550

Key words: fissionable materials; bremsstrahlung imaging; intermodal cargo containers

Abstract

The sensitivity for identification of high-Z objects in elemental form in the massive cargos of intermodal containers with continuous bremsstrahung radiation depends critically on discriminating the weak signal from uncollided photons from the very intense flux of scattered radiations that penetrate the cargo. We propose that this might be accomplished by rejection of detected events with $E \leq 2$-3 MeV that contain the majority of multiply-scattered photons along with a correction for single-scattered photons at higher energies. Monte Carlo simulations of radiographs with a 9-MeV bremsstrahlung spectrum demonstrate that rejection of detected events with $E \leq 3$ MeV removes the majority of signals from scattered photons emerging through cargos with $Z \leq 30$ and areal densities of at least145 g cm^{-2}. With analytical estimates of the single-scattered intensity at higher energies, accurate estimates of linear attenuation coefficients for shielded and unshielded uranium spheres with masses as small as 0.08 kg are found. The estimated maximum dose is generally so low that reasonable order tomography of interesting portions of a container should be possible.

1. Introduction

The possibility that clandestine fissionable material might be secreted in intermodal containers with cargo mass of up to ~ 27 Mt is recognized as a major problem for national and international security. Highly-enriched uranium (HEU) and plutonium (Pu) of relatively low masses (≤ 0.5 kg) can be detected under a wide range of cargo conditions by neutron irradiation and subsequent measurement of β-delayed high-energy γ rays following fission (ref. 1,2) The same should be possible by irradiation with very intense high-energy bremsstrahlung, and β-delayed neutrons also can be detected under some conditions with high efficiency. Nevertheless, these methods of so-called "active" interrogation will produce at least some activation of the cargo and thus are unlikely to be used as a primary means of screening of all cargo containers.

The distribution of the types, masses and container-volume averaged densities of commodities

* Corresponding author. Tel.: 510-642-5274; fax: 510-643-9685. *E-mail address:* prussin@berkeley.edu.

found in a sampling of cargo containers has been reported by Descalle, Manatt and Slaughter (ref. 3). The averaged density was found to be ~ 0.2 g cm^{-3} with less than ~ 2% at the theoretical maximum density of ~ 0.65 g cm^{-3}. The fraction of all cargos with averaged densities $\geq$ 0.4 g cm^{-3} was about 10%. Because of the known real densities of materials such as ceramics, stone products, iron and steel, organic chemicals and foodstuffs, a substantial fraction of cargos through which interrogating radiation must penetrate will have densities $\geq$ 1 g cm^{-3}.

At the present time, the only practical method for rapid screening of large cargo containers without significant activation of a cargo is by radiographic techniques using readily-available bremsstrahlung sources (see, e.g., ref. 4). Because of the need for high penetrability, such sources will likely have endpoint energies of E $\geq$ 6 MeV. The Department of Homeland Security of the United States of America (DHS) is now developing the Cargo Advanced Automated Radiography System (CAARS) for general-purpose screening of all containers. Such a system must, among other requirements, be sufficiently sensitive that it can detect cubes of high atomic number elemental material (Z $\geq$ 72) at normal densities and with a volume of 100 cm^3 behind up to 10 in. (25.4 cm) of steel anywhere in the container (ref. 5). The CAARS specifications provide that the probability for false negative signals for this case must be no more than 1 in 60 and the probability for false positive signals must be no more that 1 in 200. A 100 cm^3 volume would contain ~ 2 kg of uranium or plutonium metal. No requirements have yet been set for determining the presence of objects of arbitrary size and shape.

Even without considering the detection of arbitrary objects of high atomic number, the difficulties in approaching the CAARS requirements are formidable. The nominal dimensions of a standard intermodal cargo container are 6 - 12 m (length) x 2.4 m (height and width). Because the materials in commerce that control the average content of most cargos are composed of elements with atomic numbers Z $\leq$ 30, the mass attenuation coefficients for photons with energies in the range ~3 - 9 MeV are all very similar and can be approximated as ~ 0.032 cm^2 g^{-1} for scaling purposes (ref. 6). They are dominated by the contribution from incoherent scattering. At the maximum cargo loading, the average density is ~ 0.6 g cm^{-3}, and the fraction of incident photons in this energy range that penetrate uncolloided through the nominal width of a homogeneously-filled container is ~ 6 x 10^{-3}, the fraction that would penetrate 25.4 cm of steel uncollided is ~ 1.9 x 10^{-3}, and the fraction that would penetrate both the 25.4 cm of steel and a 4.64-cm thick cube of uranium is ~ 3.6 x 10^{-5}.

These estimates demonstrate not only that the total attenuation is expected to be very large but also, by inference, the majority of photons emerging from the container will have suffered at least one scattering event. For example, Monte Carlo simulations of the irradiation of the homogeneously-filled container considered above with a narrow 9-MeV endpoint bremsstrahlung beam (see below) show that the intensity of events from scattered photons in a thick detector, even with an energy discriminator level (E_d) of 3 MeV, is about 3 times that expected from uncollided photons alone. In the presence of an additional 25.4 cm of steel, the intensity of detected scattered events with $E_d \geq 3$ MeV is about 8 times that from uncollided photons. Thus, under a significant range of conditions expected to be found in practice, the intensity of uncollided photons that carry the spatial information needed for localization of an object of interest and for defining its attenuating characteristics will be carried by but a small fraction of the radiation emanating to a detector. While correction for scattered photons is not at

all new to radiography, the magnitude of the scattered intensity expected in cargo interrogation far exceeds that normally met with in medical and most industrial applications. We have found no publication in the open or patent literature that directly addresses this problem.

In this manuscript, we wish to demonstrate that the simple physics of Compton scattering, combined with the slowing down characteristics of highly-relativistic electrons and the general properties of the most cargos, may provide a path for development of an effective and sensitive screening mechanism for actinides in elemental form. Further, because of the relatively low total dose that must be delivered to a cargo, a procedure might be developed that is not life threatening to stowaways and allows for tomography of reasonable order in cases where such an approach would be advantageous. Because the dimensions of an object must be known if an attenuation coefficient is to be extracted, we assume that at least two orthogonal views through the container will be acquired.

2. General Theoretical Considerations

2.1 Photon Transport in Cargo

Bremsstrahlung radiation with energies significantly less than ~ 2 MeV will be much more strongly attenuated in the highly-attenuating media considered here than those of higher energy and thus will not contribute greatly to the photon spectrum emanating from a container. In the Compton limit, single incoherent interactions of 4-9 MeV photons result in scattered photons with energies less than 3 MeV when the photon scattering angle is $\theta \geq 30^0$, for which the fraction of total incoherent interactions is ≥ 0.6. Further, and neglecting photoelectric absorption, more than 85% of the photons emerging from the homogeneously-filled container described above will have suffered at least two incoherent scattering events. Thus it is reasonable to conclude that the majority of photons emerging from the container that have suffered more than a single Compton event can be suppressed by simple energy discrimination in the range ~2-3 MeV. With such discrimination, the resultant signal in an external detector will be due primarily to the desired uncollided photons and photons that have suffered but a single incoherent scattering. Given the general characteristics of the cargo fill that can be gleaned from the cargo manifest and weight, the fraction of the signal intensity due to single scattered photons should be easily estimated with the Compton scattering formalism. Along with the requirement that at least two orthogonal radiographs are acquired to provide an estimate of the dimensions of an object of interest, the ability to provide reasonable detection efficiency with sufficient spatial resolution for effective imaging rests on the spatial requirements for stopping of high-energy Compton electrons produced in an external detector.

2.2 Detector Response

The Compton electrons from scattering of photons with energies in the range 4-9 MeV at angles $\leq 30^0$ are found at angles within about 20^0 of the trajectory of the incident photons. Further, for electrons with kinetic energies in the same range, the probability for undergoing large-angle scattering before losing the majority of their kinetic energy by slowing down is small. Calculations based on the Møller scattering relation (see, e.g., ref. 7) show, for example, that the

probability of scattering at an angle of 20^o in the laboratory coordinate system is smaller by factors of about 20-25 compared to electrons of energy 0.1 MeV. Thus, the majority of the kinetic energy of most high-energy electrons produced in an external detector will be deposited in a relatively small volume about the trajectory of the incident photon. As an example, the fractions of total energy deposited within cylindrical volumes about the trajectories of incident electrons are shown in Figure 1 as functions of radial dimension and initial electron kinetic energy. These results were obtained in simulations with the code MCNP4C using the high-resolution electron transport option (ref. 8). The detector was modeled as a common plastic scintillator of composition $C_{10}H_{11}$ and density of 1.03 g cm^{-3} (ref. 9). On the average, more than 70% of the electron energy is deposited within a radial dimension $r \leq 0.8$ cm. This implies that

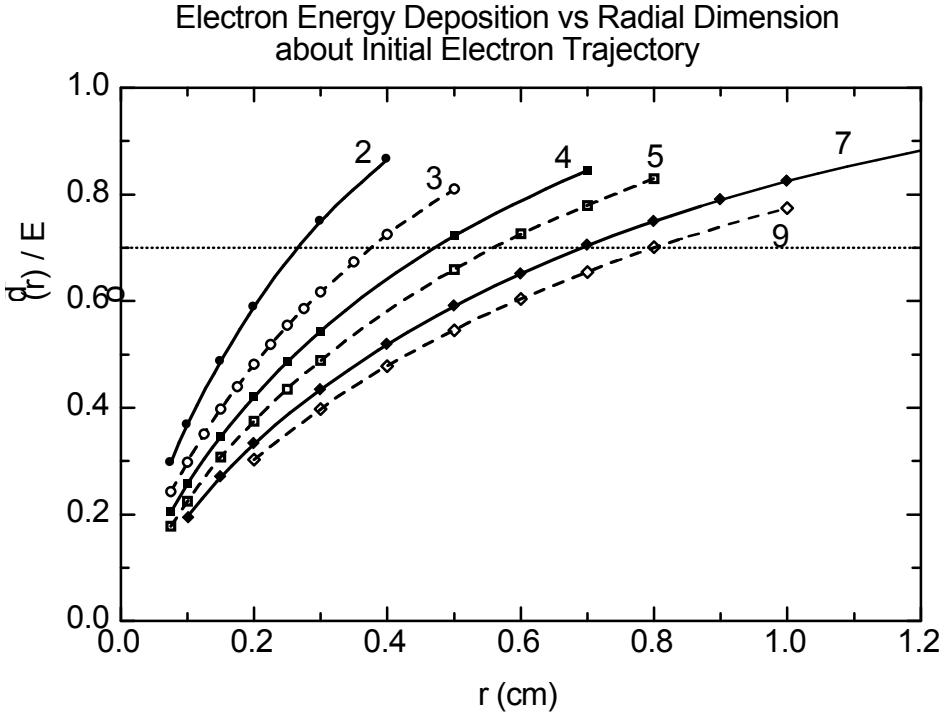

Figure 1. The fraction of electron kinetic energy deposited within a radial dimension r about the initial trajectory of an incident electron in a plastic detector (see text). The numbers adjacent to the various curves are the incident electron kinetic energies in MeV. Statistical errors in the simulations are generally within the size of the symbols.

the spatial resolution for interesting objects using a 9 MeV bremsstrahlung spectrum can be on the order of ≤ 1.5 cm in such a detector. For the common scintillators NaI(Tl) or $Bi_4Ge_3O_{12}$, the spatial resolution can be smaller by factors of ~ 1.5 - 3.0, respectively, owing to their larger electron densities, although some correction must be made for bremsstrahlung losses in the case of $Bi_4Ge_3O_{12}$.

3. Monte Carlo Simulations

The methodology outlined above has been examined with schematic simulations of a number of shielded and unshielded spheres of uranium and several other test objects. For all simulations the cargo container was assumed to have the nominal dimensions given above and was filled with water at a density of 0.6 g cm^{-3}. The bremsstrahlung spectrum was modeled from a 9 MeV electron beam interacting with a 2-cm thick tungsten target centered at 208 cm from the entrance face of the container and located on its centerline. A narrow bremsstrahlung beam was taken as that emerging from a spherical surface of 37.3 cm radius surrounding the target and collimated to provide a fan beam in the vertical direction. The horizontal width of the beam at entrance to the cargo container was 1.73 cm and diverged to 3.76 cm at entrance into the detector located immediately adjacent to the opposite face of the container at a distance of 244 cm. For some simulations a wide beam 18.2-cm in width was produced by translating the narrow beam in horizontal steps of 1.5 cm.

As discussed above, the detector was modeled as a plastic scintillator with dimensions of 50 cm (height) x 50 cm (width) and 6" (15.4 cm) thickness. Photon interactions were allowed to occur throughout the detector volume and electron transport was used to define the total energy deposited in various interaction volumes. To simulate the response of a pixilated detector, the detector surface was divided into an array of 1.5 cm x 1.5 cm areas. The energy deposited in a detector pixel was defined as that deposited in the volume swept by projecting the pixel surface through the detector. The response of a more realistic scintillator comprised of individual parallelepipeds separated by lead foils sufficiently thick to prevent transmission of electrons, scintillation light and low-energy bremsstrahlung was shown by simulations to provide essentially the same results for high energy radiations although the total count rates were reduced by about a factor of 2. The total average attenuation of 3-9 MeV photons traversing the thickness of the detector was ~ 0.35. The detector efficiency per bremsstrahlung source photon was obtained by direct comparison of the intensities in pixels in the absence of a target and with and without the water fill. This efficiency was used to normalize the results from the simulations to the results from the first Compton scatter calculations.

The thrust of all simulations and analyses presented here is to judge the efficacy of the proposed approach for providing high-quality linear attenuation coefficients from which detection of high-Z fissionable materials can be ascertained in massive cargos. For this purpose, it is assumed that the dimensions of an object are known and that the only errors are those due to the estimated statistical errors inherent in the simulated intensities in the detector pixels.

3.1 Test of the Concept

A simple test of the general concept outlined above was obtained by the simulation of a 2-cm radius totally absorbing sphere located at the center of the filled cargo container that is interrogated by the narrow bremsstrahlung beam defined above. The intensities (lineouts) of events per source photon in the vertical line of pixels passing through the centerline of the target are shown as a function of discrimination energy in Figure 2. As the threshold level is raised from 1 eV to 3 MeV, the intensity in non-target and target pixels decreases by a factor of about 7-8 and 55, respectively. In Figure 3 are shown the effective linear attenuation coefficients as a function of discrimination energy as estimated in the normal manner by calculating the quantity

$$\mu_{\text{eff}} = \frac{1}{x_{\text{obj}}} \ln \frac{I'}{I} \qquad (1)$$

where I' is the average intensity in a non-target pixel and I is the intensity in the central target pixel.

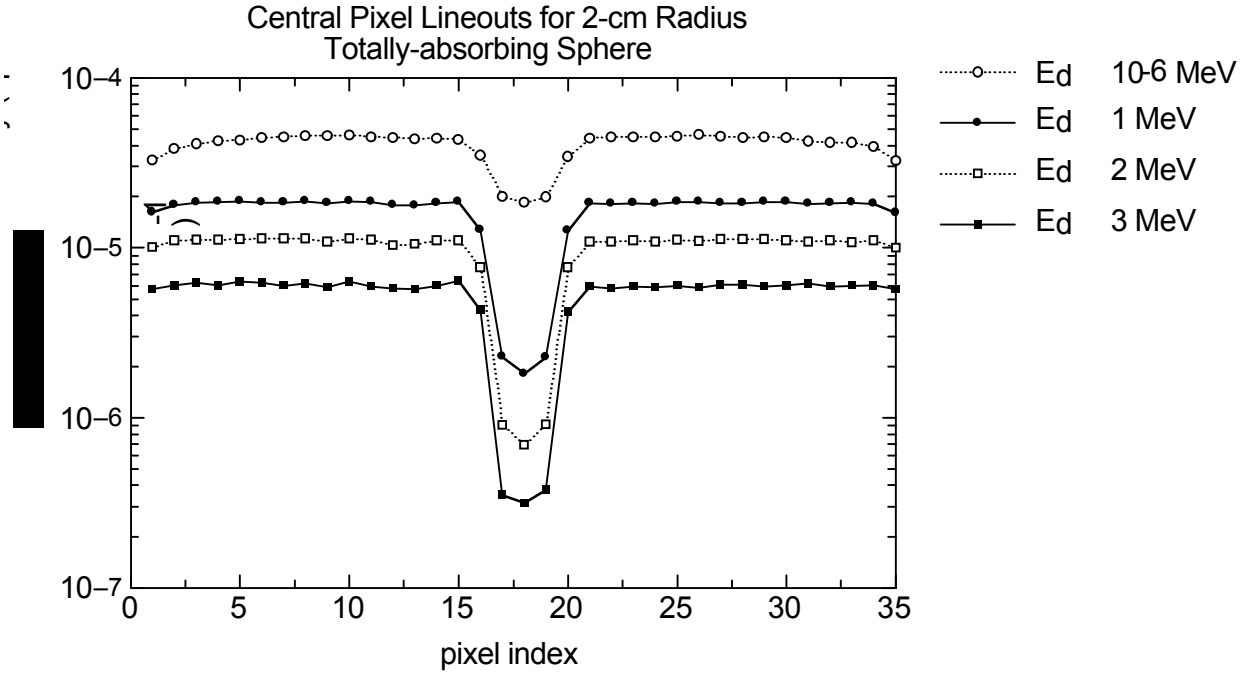

Figure 2. Intensities (lineouts) in the vertical column of pixels along the centerline of a 2-cm radius totally absorbing sphere located at the center of cargo container filled homogeneously with water at a density of 0.6 g cm^{-3}.

The calculated μ_{eff} are seen to increase by a factor of about 3 as the discrimination level is raised from about 1 eV to about 3 MeV. The error bars shown represent only the 1 σ statistical uncertainties in I and I' estimated in the Monte Carlo simulations. The lower limit indicated by the underlined arrow represents the μ_{eff} obtained by applying the analytical estimate of the first-Compton scattering intensity with the procedure outlined in the Appendix. Within the statistical errors, the resultant μ_{eff} is consistent with the infinite value expected.

This simple test supports the central ideas that, in the main, energy discrimination removes the majority of multiple-scattered incident photons and that the remaining scattered intensity can be estimated reasonably well from the simple physics of Compton scattering. These conclusions are further supported by analytical considerations and other simulations with the homogeneously-filled container in the absence of a target. In particular, the strong dependence of the energy of scattered photons on the scattering angle means that high-energy scattered photons reaching a

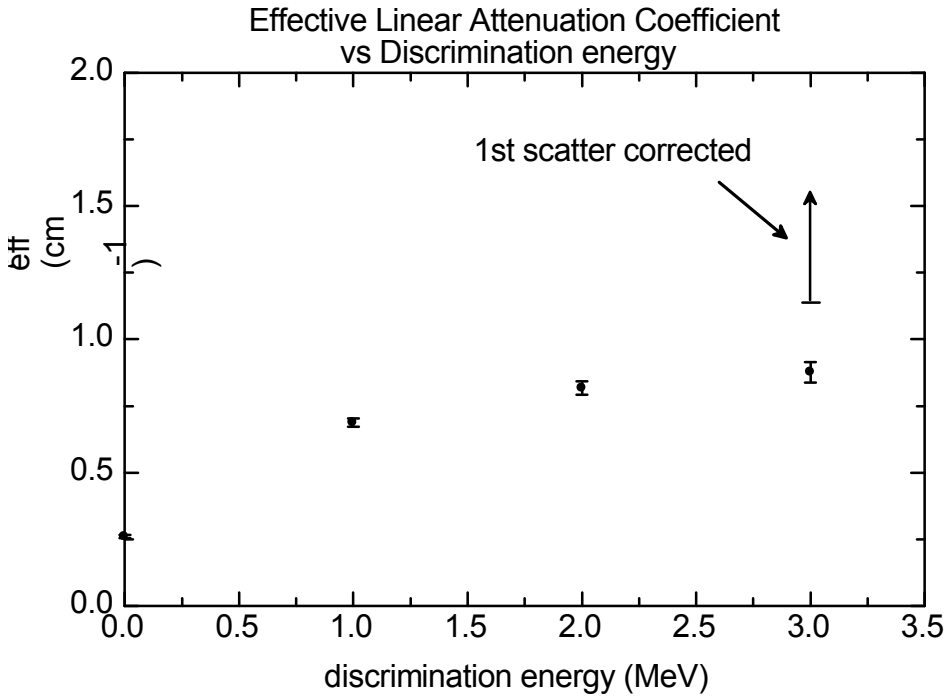

Figure 3. Effective linear attenuation coefficient, μ_{eff}, extracted from the Monte Carlo simulations shown in Figure 2 as a function of detector discrimination level.

target pixel can only arise from interactions that take place within a fairly small transverse dimension about the incident photon's trajectory.

3.2 Simulations of Shielded and Unshielded Uranium and Rhodium Spheres.

The methodology discussed here has been applied to simulations of an array of targets, including uranium spheres with radii of 1, 2 and 3 cm, a 2-cm radius uranium sphere contained within 2-cm thick spherical shells of iron and lead, and a 2-cm sphere of rhodium, the element with the largest linear attenuation coefficient outside of the actinides. The smallest uranium sphere represents a case for which the object is comparable in size to the pixel dimension while the largest uranium sphere approaches that of a totally absorbing object. The Monte Carlo simulations were performed in the same manner as described in Section 3.1, i.e., all targets were located at the center of a cargo container that was otherwise filled with water at 0.6 g cm^{-3}. In the case of the 3-cm radius sphere of uranium, the water contained in the 25.4-cm thick slab immediately adjacent to the beam entrance was replaced by the same thickness of iron in order to provide a simulation somewhat more stringent than that specified in the DHS requirements discussed in Section 1.

In all cases, μ_{eff} of the object of interest was calculated from equation (1) using the simulated intensities with a 3 MeV discrimination level. The intensity I was taken as that in the central target pixel and the intensity I' was taken as the average intensity in the five non-target pixels

just removed from the target region, both intensities corrected for scattering above the discriminator level with the model given in the Appendix. For simplicity, it was assumed that the object itself was totally absorbing in applying the scattering model. With the exception of the case of a uranium sphere shielded in a spherical shell of iron discussed further below, this approximation is reasonable but somewhat conservative. No corrections were made for the divergence of the bremsstrahlung beam that leads to magnification of the target in the detector plane.

The total target thickness penetrated by unattenuated photons that interact in the central target pixel was taken as the mean cord length through a sphere over the pixel width. To compare the derived μ_{eff} with those expected, spline fits to tabular values of μ/ρ from ref. 6 were averaged over the simulated bremsstrahlung spectrum in the energy range 3-9 MeV and then multiplied by the normal density of the element. For shielded spheres, the μ_{eff} derived in this way were again averaged by the mean cord lengths through the spherical cores and spherical shells.

As examples, the intensities from the vertical columns of detector pixels that contain the central targets pixels for simulations of a 2-cm radius sphere of uranium contained in 2-cm thick spherical shells of iron and lead are shown in Figure 4. For these simulations the 18.2 cm wide beam was used. In both cases, the increase in detector threshold energy from 0.1 keV to 3 MeV

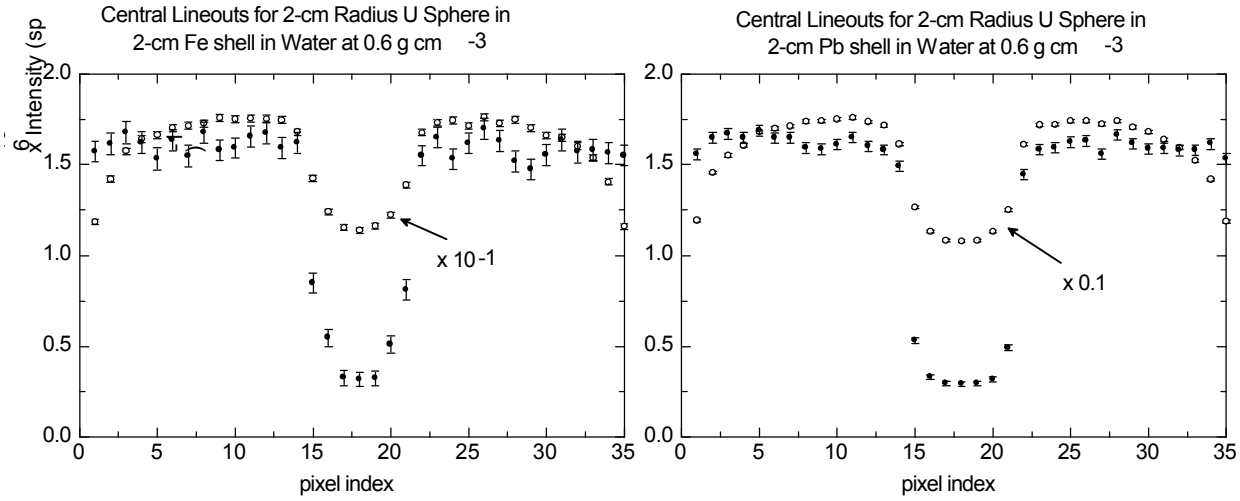

Figure 4. Intensities in vertical column of pixels containing the central target pixel for a 2-cm radius sphere of uranium inside of a 2-cm thick spherical shell of iron (left panel) and inside of a 2-cm thick spherical shell of lead (right panel). The vertical axes of the two panels are identical. Open circles - 0.1 keV detector threshold. Closed circles - 3 MeV detector threshold. Errors bars represent the estimated 1σ statistical uncertainty in the simulation only.

reduces the intensities in non-target pixels by about a factor of 10 while the intensities in the central target pixels are reduced by about a factor of 40. Although both targets have the same

dimensions, that for the iron-shielded uranium sphere appears to be significantly smaller in the vicinity of the central target pixel than that of the lead-shielded sphere due to the rather high transparency of the outer 1 cm of the iron. Also evident is the magnification of the target in the detector plane because of the divergence of the bremsstrahlung beam.

The simulation of the 3-cm radius uranium sphere in the presence of a 25.4-cm thick slab of iron at the beam entrance to the container is shown in Figure 5. Again the wide beam was used in the simulation. The strong attenuation by the iron slab is immediately evident, the intensities in non-target pixels being smaller by a factor of about 130 compared to the intensities seen in Figure 4 when the detector discrimination level is 3 MeV. Nevertheless, and notwithstanding the fact that the iron also acts as a very strong scattering source, the uranium sphere is quite well visualized. While the statistical quality of the simulation is poorer because of computational limitations, the ratio of the average intensity in non-target pixels to that in the central target pixels is essentially

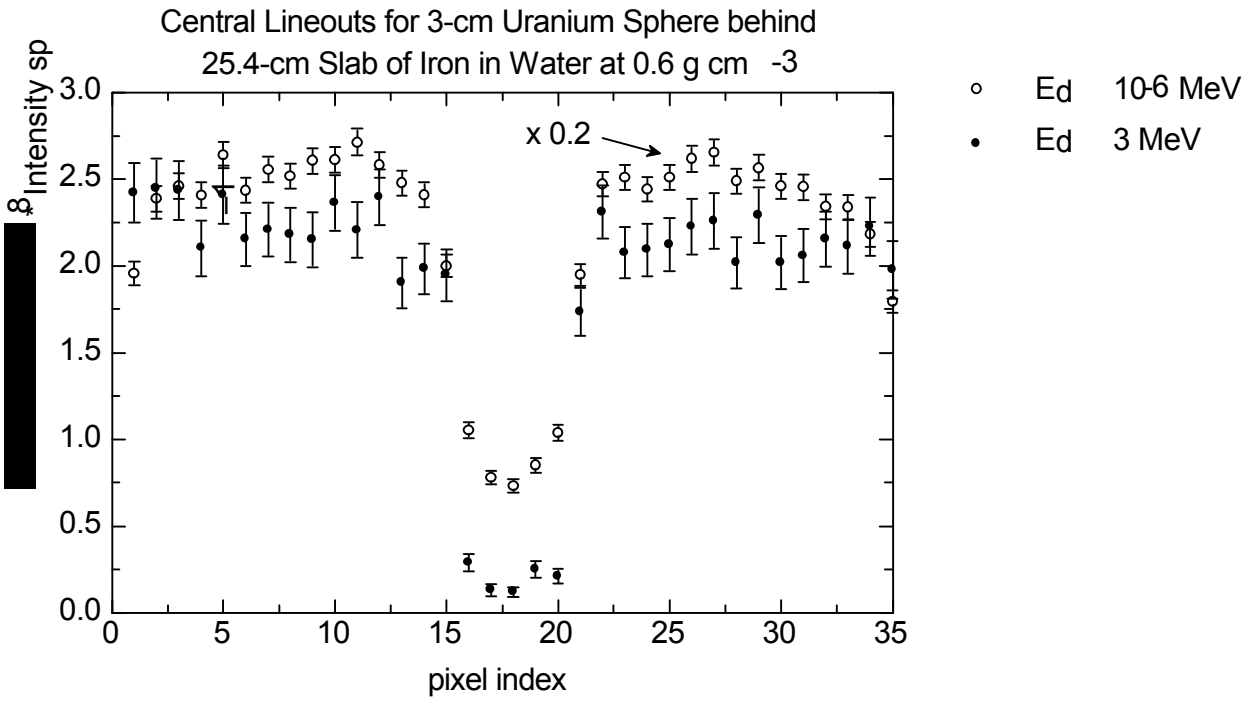

Figure 5. Intensities in the vertical column of pixels containing the central target pixel for a 3-cm radius sphere of uranium behind a 25.4-cm thick slab of iron with the remainder of the container filled with water at a density of 0.6 g cm^{-3}. Errors bars represent the estimated 1σ statistical uncertainty in the simulation only.

identical to that seen in Figure 2 for the totally absorbing sphere as it should be. A 3-cm radius sphere of uranium is very nearly totally absorbing to 3-9 MeV photons. This indicates, at least qualitatively, that the addition of a strong scattering source does not greatly change the relative intensity of high-energy photons that scatter into the target pixels.

A summary of the principal parameters from 7 of the simulations considered in this work is given in Table 1 and the μ_{eff} extracted from the simulations and the first scattering model are compared to those expected from the attenuation properties of the target in Figure 6. As seen in the summary and the figure, the application of energy discrimination, coupled with the first Compton scatter estimates that assume the target to be totally absorbing, lead to linear attenuation coefficients that agree with the expected values to within about 1 σ except for case c. As discussed previously (see Figure 4), the outer portion of the iron shield is relatively transparent to the high-energy photons considered here. Simple analytical estimates show, for example, that the transmission of the outer 1 cm of the iron to photons in the energy range 3-9 MeV is about 0.4. Because first scatterings that result in photons near the source energy are produced only at small scattering angles, this transparency has a significant effect on the intensity of the first scattering estimate. Indeed, an approximate calculation that includes this transparency brings the extracted μ_{eff} well within the 1 σ limits of a one-to-one correspondence with the expected value.

Table 1. Summary of principal parameters of 7 simulations used to test the efficacy of the energy discrimination plus first scattering model approach.

target	thickness[d] (cm)	$\mu_{expected}$ (cm^{-1})	μ_{eff} (cm^{-1})[b]	μ_{eff} / $\mu_{expected}$
water cargo	244.000	0.020[c]	0.020 ± 0.003	1.00 ± 0.15
Rh sphere (r = 2 cm)	3.369	0.467	0.463 ± 0.022	0.991 ± 0.047
U sphere (r = 2 cm) in 2-cm thick Fe shell[a]	5.333	0.549	0.435 ± 0.067[a]	0.792 ± 0.122[a]
U sphere (r = 2 cm) in 2-cm thick Pb shell	5.333	0.603	0.524 ± 0.079	0.869 ± 0.131
U sphere (r = 2 cm)	3.369	0.851	0.892 ± 0.057	1.048 ± 0.067
U sphere (r = 3 cm) + 25.4-cm thick Fe slab	4.000	0.850	0.801 ± 0.271	0.942 ± 0.319
U sphere (r = 1 cm)	1.684	0.851	0.764 ± 0.093	0.898 ± 0.109

[a] uncorrected for transparency through outer portion of the iron shell. See text.
[b] uncertainties due solely to estimated statistical uncertainties in the Monte Carlo intensities.
[c] for water at a density of 0.6 g cm^{-3}.
[d] mean thickness of target averaged over the dimension of the central pixel.

4. Discussion

The simulations and analysis presented above suggests that it is indeed possible to determine the linear attenuation coefficient of isolated objects of normal elemental density with sufficient accuracy that a reliable and efficient screening procedure might be developed based on a single endpoint energy bremsstrahlung beam. The fundamental issue is the ability to distinguish between high-Z objects that might contain fissionable material and lower atomic numbers within

the limits for false positive and false negative signals desired by the DHS. In Figure 6 are shown approximate limits for the false positive and false negative detection rates specified for CAARS calculated with rough estimates of uncertainties in the attenuation coefficient of the cargo and the dimensions of an object. With the exception of some shielding conditions, both limits might be met with detailed development of the proposed methodology. Although not presented here, it may be completely possible to improve the identification of high-Z objects by analysis of various energy ranges of the detected events.

The majority of the simulations were performed with about10^8 histories. Commercial bremsstrahlung sources can produce roughly 10^{12} photons s^{-1}. Assuming that general purpose scanning must be accomplished in about 1 min, a 40' (12.2 m) cargo container, and a beam width on the order of 10 cm, the maximum count rates in an individual pixel would be less than about 5 x 10^4 s^{-1}. Such rates should permit energy discrimination in the detection system with standard electronics and techniques. For objects such as the 3-cm radius sphere of uranium shielded by 25.4 cm of iron, which required 10^{10} histories to produce the statistical quality shown in Figure 5, it is assumed that much longer data acquisition times will be permitted if warranted. Further, a reasonable number of angular projections can be acquired in a relatively short time where they might prove useful to better define the attenuation characteristics of suspect objects in cluttered environments.

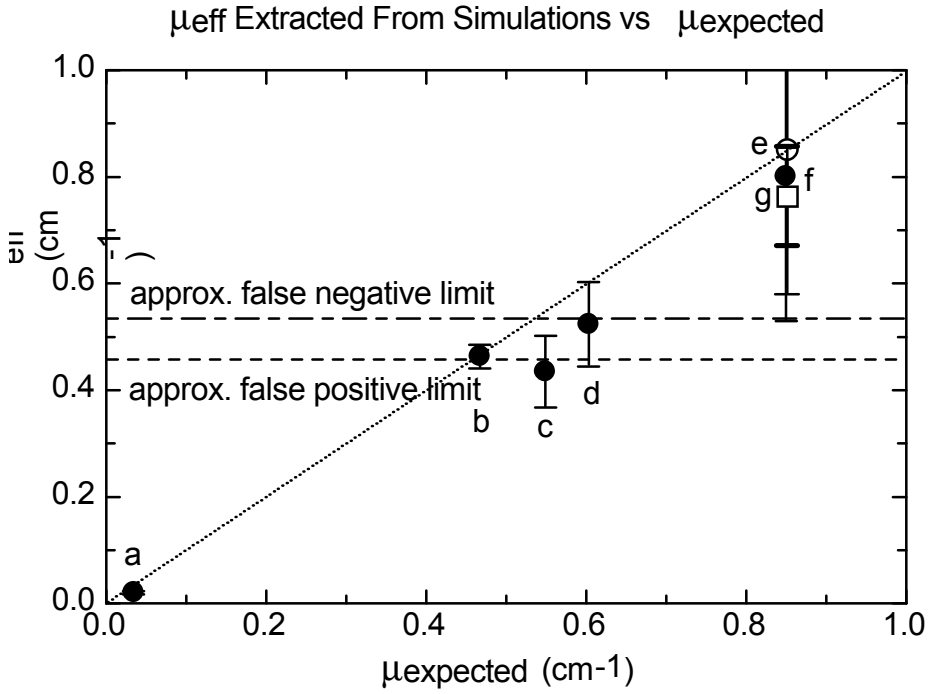

Figure 6. The μ_{eff} extracted from the Monte Carlo simulations and the first Compton scattering correction versus the expected linear attenuation coefficient. All simulations assume that targets are located at the center of a cargo container otherwise filled homogeneously with water at a density of 0.6 g cm^{-3}. Errors bars represent the estimated 1σ statistical uncertainty in the simulation only. a- water cargo; b - Rh sphere (r = 2 cm);

c - U sphere (r = 2 cm) in 2-cm thick Fe shield; d - U sphere (r = 2 cm) in 2-cm thick Pb shield; e - U sphere (r = 2 cm); f - U sphere (r = 3 cm) + 25.4-cm thick Fe slab; g - U sphere (r = 1 cm).

The dose that might be received by a human during scanning was estimated with a crude phantom model in the case where 10^8 histories were simulated. If a person were stationary in the container, the whole body dose was estimated to be roughly 200 mrad. If the individual traversed the container along with the bremsstrahlung beam, the estimated dose was about 2 rad.

The quality of the linear attenuation coefficients estimated in this work was somewhat compromised by the simplicity of the implementation of the first scattering model. Nevertheless they should be illustrative of what might be expected in practice for isolated objects in a container with a homogeneous cargo fill. Because of the makeup of most cargos, and assuming that the cargo manifest and weight are known, it should be possible to obtain a reasonable estimate of the effective density and attenuation coefficient of the cargo from the two orthogonal radiographs assumed here. Our experience with photon transport in a similar energy range for examining the use of delayed γ rays for detecting fissionable materials has shown that apart from significant streaming paths, the requirement of homogeneity should not be a serious limitation. Whether cargo clutter will be a significant limitation and whether there is any hope of distinguishing non-elemental objects containing actinides still awaits study.

Finally, we wish to point out that unequivocal definition of the presence of fissionable material can be obtained by irradiation of the cargo container with higher-energy photons or with neutrons with energies ≥ 7 MeV by detecting high-energy β-delayed γ-ray emission. This could be attained with the same detector system as envisioned here with a dual-purpose interrogation system. This would provide a very powerful deterrence against the secretion clandestine nuclear materials in cargo containers.

5. Appendix: First Scattering Approximation

In Figure A.1 is shown a schematic of a cargo container from which the first scattering approximation is derived. The width of the container is z_o. Pixels associated with the position of an interesting object are contained within the dimension $0 \leq x_t \leq w$. The container is irradiated with bremsstrahlung photons incident normally on the container side opposite to the detector . We consider here only the first scatterings of bremsstrahlung photons that are incident on the detector plane over the dimension $w \leq x \leq x_o$.

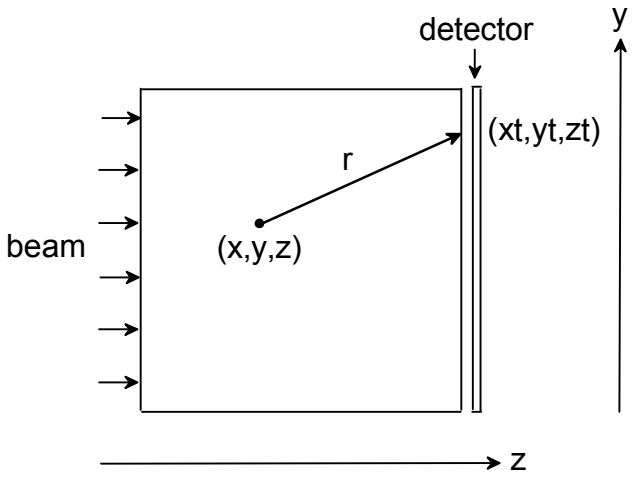

End view

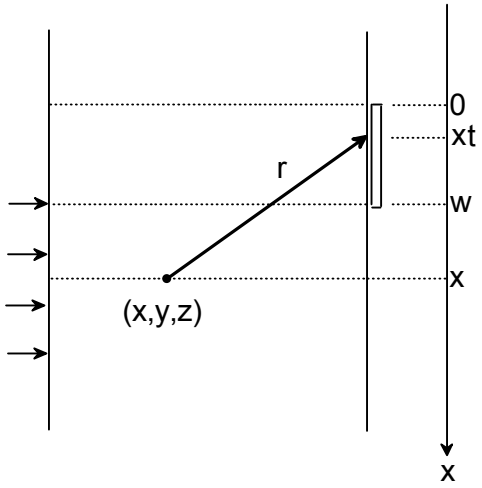

Top view

Figure A.1 End and top views of the geometry used for derivation of the expression for calculating the intensity of events from single Compton scattering of monoenergetic photons incident on the cargo container volume.

Photons of intensity I_o cm^{-2} are incident at the location x, y, z = 0, interact at the location x,y,z by Compton scattering, and produce scattered photons that are directed along the trajectory r to a point x_t,y_t,z_t in the detector plane. The magnitude of r is $r = \left[(x-x_t)^2 + (y-y_t)^2 + (z-z_t)^2\right]^{1/2}$.

The electron density is n_e cm^{-3} and the differential Compton collision cross section for unpolarized photons is ${}_e\sigma_C(\theta)$ cm^2 str^{-1}. With normal Cartesian and polar coordinate systems, where θ is the polar angle and ϕ is the azimuthal angle, the element of solid angle between θ and

445 ($\theta + d\theta$) and $\phi + (\phi + d\phi)$ is $d\omega = \sin\theta d\theta d\phi$ and the surface area subtended by this solid angle is
446 $dS = r^2 d\omega$. The total rate of scattering events from photons incident in the differential area dA
447 about the location (x, y, z = 0) that interact between z and (z + dz) and produce photons scattered
448 into $d\omega$ is
449
450 $$n_e I_o e^{-\mu z} \sigma_C(\theta) dA_e dz d\omega \text{ s}^{-1} \quad \text{(A.1)}$$
451
452 The flux of unattenuated first-scattered photons at the point (x_t, y_t, z_o) produced from these
453 events is then
454
455 $$d\phi = \frac{e^{-\mu r}}{r^2} I_o e^{-\mu z} dA_e \sigma_C(\theta) \cos(\theta) n_e dz \text{ cm}^{-2} \text{ s}^{-1}, \quad \text{(A.2)}$$
456
457 where the factor $\cos(\theta)$ represents the projection of dS onto the plane surface of the detector.
458 The total flux of first-scattered photons per unit intensity I_o at (x_t, y_t, z_o) due to interactions along
459 the range $0 \le z \le z_o$ is then
460
461
462 $$\frac{d\phi}{I_o dA} = n_e \int_0^z \frac{e^{-\mu r}}{r^2} e^{-\mu z}{}_e \sigma_C(\theta) \cos(\theta) dz, \quad \text{(A.3)}$$
463
464 where $e^{-\mu r}$ accounts for attenuation of the scattered photons along the trajectory r. The energy
465 spectrum of the photons arriving at the detector plane is readily obtained from the normal
466 Compton relation
467
468 $$E'(\theta) = \frac{E_o}{1 + \frac{E_o}{m_e c^2}(1 - \cos(\theta))}, \quad \text{(A.4)}$$
469
470 where E_o and $E'(\theta)$ are the energies of the incident photon and scattered photon, respectively
471 and m_e is the rest mass of the electron.
472
473 In the implementation used here, the incident photons were assumed to be normal to the face of
474 the cargo container and no account was taken for the divergence of the beam. Intensities of
475 scattered photons from incident monoenergetic photons incident over the range $0 \le x \le w$ were
476 calculated only at the center of 1 cm x 1 cm pixels located at the front face of the detector ,
477 weighted for the intensity distribution of the bremsstrahlung spectrum and then normalized to
478 the Monte Carlo simulations by use of the simulated efficiency for photon detection. Further, it
479 was assumed that the target was totally absorbing and thus the first scattered intensity will be
480 underestimated to some extent.
481
482
483 References
484

1. E.B. Norman, S.G. Prussin, R-M Larimer, H. Shugart, E. Browne, A.R. Smith, R.J. McDonald, H. Nitsche, P. Gupta, M.I. Frank, T.B. Gosnell, Nucl. Instrum. & Methods A **521** (2004) 608.

2. S.G. Prussin, M-A. Descalle, J.M. Hall, J.A. Pruet, D.R. Slaughter, M.R. Accatino, O.J. Alford, S.J. Asztalos, A. Bernstein, J.A. Church, T. Gosnell, A. Loshak, N.W. Madden, D.R. Manatt, G.J. Mauger, A.W. Meyer, T.L. Moore, E.B. Norman, B.A. Pohl, D.C. Petersen, B. Rusnak, T.B. Sundsmo, W.K. Tenbrook, R.S. Walling, Nucl. Instrum. & Methods A **569** (2006) 853.

3. M.-A. Descalle, D. Manatt and D. Slaughter, Lawrence Livermore Laboratory report UCRL-TR-225708 (2006).

4. Varian Medical Systems, Security and Inspection, 6883 Spencer Street, Las Vegas, NV 89119.

5. CAARS Performance Specifications - Response to Vendors Comments, U.S. Dept. of Homeland Security, Domestic Nuclear Detection Office, Document Number DNDO PS-100380v3.00, February 2006

6. M.J. Berger,[1] J.H. Hubbell,[1] S.M. Seltzer,[1] J. Chang,[2] J.S. Coursey,[2] R. Sukumar,[2] and D.S. Zucker[2], XCOM: Photon Cross Sections Database, NIST Standard Reference Database 8 (XGAM), U.S. Dept. of Commerce, 1998.

7. M.B. Scott, A.O. Hanson, E.M. Lyman, Phys. Rev. **84** (1951) 638.

8. J.F. Briesmeister. MCNP—A General Monte Carlo N-Particle Transport Code Version 4C, Los Alamos National Laboratory (2000).

9. Eljen Technology, 2010 E. Broadway, Sweetwater, Texas 79556.

This work was performed under the auspices of the U. S. Department of Energy by University of California, Lawrence Livermore National Laboratory under Contract W-7405-Eng-48.